Progress In Electromagnetics Research Letters, Vol. 51, 79–85, 2015

A Novel Compact Dual-Wideband Bandpass Filter with Multi-Mode Resonators

Jun Li[1, 2, *], Shan-Shan Huang[1, 3], Hui Wang[4], and Jian-Zhong Zhao[1]

Abstract—A novel compact dual-wideband bandpass filter (BPF), with two multi-mode resonators (MMRs), a quad-mode one (QMR) and a triple-mode one (TMR), is proposed in this paper. The first passband is generated by a QMR loaded with a short-ended stub and two open-ended stubs, and the second one is realized by a TMR loaded with a square ring and a short-ended stub. Each passband can be tuned separately by controlling the corresponding resonator. The classical even-/odd-mode analysis is applied to characterize the presented MMRs due to their symmetric configurations. In order to validate the design methodology, a dual-wideband BPF prototype centered at 2.34 and 3.46 GHz with fractional bandwidths of 25.6% and 21.4% for WLAN and WiMAX applications is designed, fabricated and measured. Measurements have good agreement with simulations.

1. INTRODUCTION

In the last decades, dual-band bandpass filters (BPFs) have been aggressively investigated due to the rapid development of modern multi-band multi-service wireless communication systems. As a result, various dual-band BPFs have been reported [1–7]. For example, stepped-impedance resonators (SIRs) are employed to design a dual-band BPF in [1]. In [2] quarter-wavelength SIR is used to implement dual-band BPF. A tri-band BPF using asymmetric SIR with one step discontinuity is proposed in [3]. However, the center frequencies cannot be independently controlled. By utilizing two pairs of degenerate modes of a single ring resonator, dual-band response is achieved in [4]. However, this solution needs indispensable perturbations and suffers from notch-like upper stopband. Dual-band BPF, which resonant frequencies can be controlled by tuning the centrally loaded stubs, is realized by stub-loaded resonators in [5]. In [6], center-grounded SIRs are introduced to design dual-band filter. Multi-mode resonators (MMRs) are proposed to implement dual-band BPFs in [7]. Although these filters are qualified for some applications, the bandwidths of these filters are not wide enough to satisfy the requirement in modern dual high data-rate communication systems. Thus, dual-wideband BPFs are needed. Recently, some dual-wideband BPFs have been reported [8–11]. Short-circuited SIRs [8], transversal signal-interaction concept [9], open stub-loaded coupled-line section [10], and penta-mode resonator [11] are introduced to implement dual-wideband BPFs. However, only a few designs of high performance dual-wideband BPFs have been reported so far.

In this letter, a novel compact dual-wideband BPF with two MMRs is proposed. The first MMR is a quad-mode resonator (QMR) which consists of a main transmission line loaded with a short-ended stub and two open-ended stubs, and the second MMR is a triple-mode resonator (TMR) which is composed of a main transmission line loaded with a square ring and a short-ended stub. Even-/odd-mode analysis is applied to explain their resonant characteristics due to their symmetric configurations.

Received 23 December 2014, Accepted 22 January 2015, Scheduled 30 January 2015

* Corresponding author: Jun Li (lijun_njust@163.com).

[1] Ministerial Key Laboratory of JGMT, Nanjing University of Science and Technology, Nanjing 210094, China. [2] Huawei Technologies Co., Ltd., Shanghai 200121, China. [3] Spreadtrum Communications Inc., Shanghai 201203, China. [4] 28th Research Institute of China Electronics Technology Group Corporation (CETC), Nanjing 210007, China.

By arranging the four and three resonant modes of the QMR and TMR within the desired passbands, and then connecting the two resonators with a common short-ended via-hole and feeding them with a pair of common feedlines, the proposed dual-wideband BPF is constituted. The center frequency (CF) and bandwidth of each passband can be tuned separately by controlling the corresponding resonator. Finally, the design method is verified by a fabricated prototype filter, and the measured results agree well with the simulated ones.

2. DUAL-WIDEBAND BPF DESIGN

2.1. Analysis of the Proposed MMRs

Figure 1(a) illustrates the specific configuration of the QMR which generates the first passband. As can be seen in Figure 1(a), it consists of a main transmission line loaded with a short-ended stub and two open-ended stubs. For analysis simplicity, the widths of the main transmission line and the loaded open-ended stubs are w, whereas the width of the loaded short-ended stub is $2w$. In addition, the condition with $\theta_1 = \theta_2 = \theta = \pi/2$ at frequency f_{m1} is considered in this section, where $\theta_n = 2\pi L_n/\lambda_g$ $(n = 1, 2, s, s_1)$ and λ_g is the guided wavelength at f_{m1}. Since the QMR is symmetric in structure, even-/odd-mode analysis can be adopted to characterize it.

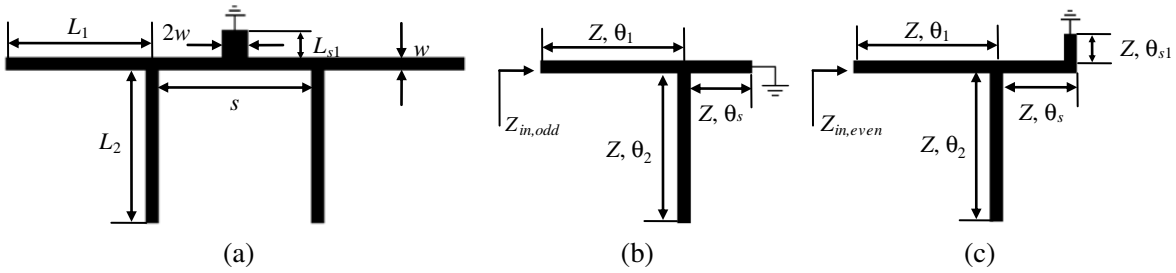

Figure 1. (a) Configuration of the QMR, (b) odd- and (c) even-mode equivalent circuits of (a).

For the odd-mode excitation, the symmetrical plane is equivalent to an electric wall, and Figure 1(b) depicts its equivalent circuit. The one-port input impedance of the odd-mode equivalent circuit is

$$Z_{in,\,odd} = jZ\frac{\tan^2\theta - \cot\theta_s\tan\theta - 1}{2\tan\theta - \cot\theta_s} \tag{1}$$

The odd-mode resonance occurs when $Z_{in,\,odd} = \infty$, which is

$$\tan\theta = \infty \tag{2a}$$

$$2\tan\theta - \cot\theta_s = 0 \tag{2b}$$

By solving Equation (2), the odd-mode resonant frequencies of the QMR can be obtained as

$$f_{o1} = f_{m1} \tag{3a}$$

$$f_{o2} = \frac{2f_{m1}}{\pi}\tan^{-1}\left[\frac{\cot\left(s\pi/\lambda_g\right)}{2}\right] \tag{3b}$$

For the even-mode excitation, the symmetrical plane can be modeled as a magnetic wall, and its equivalent circuit is illustrated in Figure 1(c). The input impedance of the even-mode equivalent circuit is

$$Z_{in,\,even} = jZ\frac{\tan^2\theta - \cot\left(\theta_s + \theta_{s1}\right)\tan\theta - 1}{2\tan\theta - \cot\left(\theta_s + \theta_{s1}\right)} \tag{4}$$

By applying the even-mode resonant condition $Z_{in,\,even} = \infty$, the following equations can be obtained

$$\tan\theta = \infty \tag{5a}$$

$$2\tan\theta - \cot\left(\theta_s + \theta_{s1}\right) = 0 \tag{5b}$$

Thus, the even-mode resonant frequencies of the QMR can be expressed as

$$f_{e1} = f_{m1} \tag{6a}$$

$$f_{e2} = \frac{2f_{m1}}{\pi}\tan^{-1}\left[\frac{\cot\left(\left(s+2L_{s1}\right)\pi/\lambda_g\right)}{2}\right] \tag{6b}$$

From Equations (3) and (6), one can clearly observe that the QMR generates four resonant modes (i.e., f_{o1}, f_{o2}, f_{e1}, and f_{e2}). However, $f_{o1}(f_{e1})$ is a degenerate mode. According to [4], the degenerate mode will split when a perturbation is used. Thus, the presented QMR exhibits quad-mode resonant characteristics when the two open-ended stubs are weakly coupled to each other as a perturbation. In addition, Equation (3b) reveals that f_{o2} is only affected by s, whereas Equation (6b) indicates that L_{s1} only influences f_{e2}. Therefore, it is possible to build up a passband with wide bandwidth when the four modes draw near. That is, when s and $s+2L_{s1}$ is short enough, f_{o2} and f_{e2} will approach to f_{m1} according to Equations (3b) and (6b) respectively, then the first wideband can be constructed.

Figures 2(a) and (b) depict the extracted resonant modes of the QMR with varied L_{s1} and s. It is clear that f_1 can be controlled by L_{s1} independently and both f_1 and f_2 are affected by s. In addition, f_3 and f_4 get closer when s becomes longer. This is because, when s increases the coupling between the two open-ended stubs becomes weaker, and the two modes tend to merge as one degenerate mode. The conclusions drawn from these two plots are consistent with the analysis mentioned above.

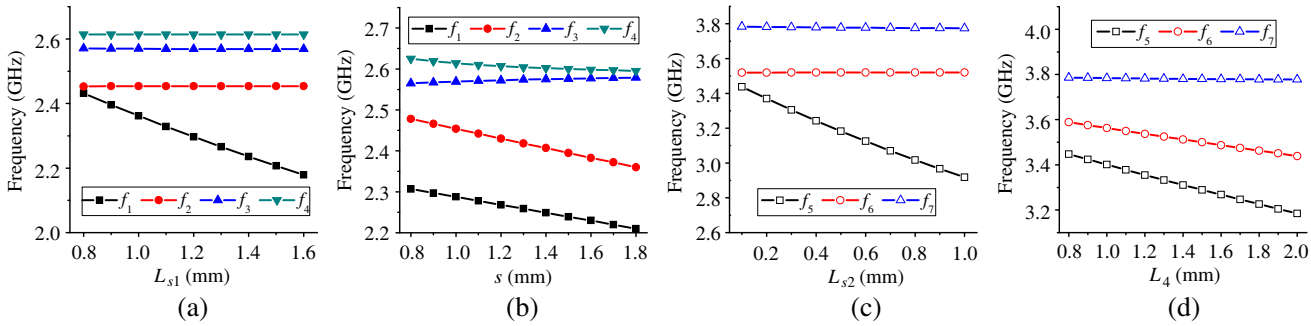

Figure 2. Variation of resonant modes with varied (a) L_{s1} ($w = 0.4$, $L_1 = L_2 = 18.15$, $s = 1$), and (b) s ($w = 0.4$, $L_1 = L_2 = 18.15$, $L_{s1} = 1.23$) of the QMR, and variation of resonant modes with varied (c) L_{s2} ($w = 0.4$, $L_3 = L_5 = 12.25$, $L_4 = 1.34$), and (d) L_4 ($w = 0.4$, $L_3 = L_5 = 12.25$, $L_{s2} = 0.23$) of the TMR. Unit: mm.

The specific configuration of the TMR is depicted in Figure 3(a). It provides the second passband. As shown in Figure 3(a), it consists of a main transmission line loaded with a square ring and a short-ended stub. For analysis simplicity, the widths of the main transmission line and the loaded square ring are w, whereas the width of the loaded short-ended stub is $2w$. In addition, the condition with $\theta_3 = \theta_5 = \theta = \pi/2$ at frequency f_{m2} is considered in this section, where $\theta_n = 2\pi L_n/\lambda_g$ ($n = 3, 4, 5, s_2$) and λ_g is the guided wavelength at f_{m2}. Even-/odd-mode analysis method can be applied to explain its resonant characteristics due to its symmetrical configuration.

The one-port input impedance of the odd- and even-mode equivalent circuits shown in Figures 3(b) and (c) can be derived as

$$Z_{in,\,odd} = jZ\frac{\cot\theta_4\tan\theta + 2}{\cot\theta - \tan\theta + \cot\theta_4} \tag{7a}$$

$$Z_{in,\,even} = jZ\frac{\tan^2\theta - \cot\left(\theta_4+\theta_{s2}\right)\tan\theta - 1}{2\tan\theta - \cot\left(\theta_4+\theta_{s2}\right)} \tag{7b}$$

By applying the resonant conditions $Z_{in,\,odd} = \infty$ and $Z_{in,\,even} = \infty$, the following equations can be obtained

$$\tan^2\theta - \cot\theta_4\tan\theta - 1 = 0 \tag{8}$$

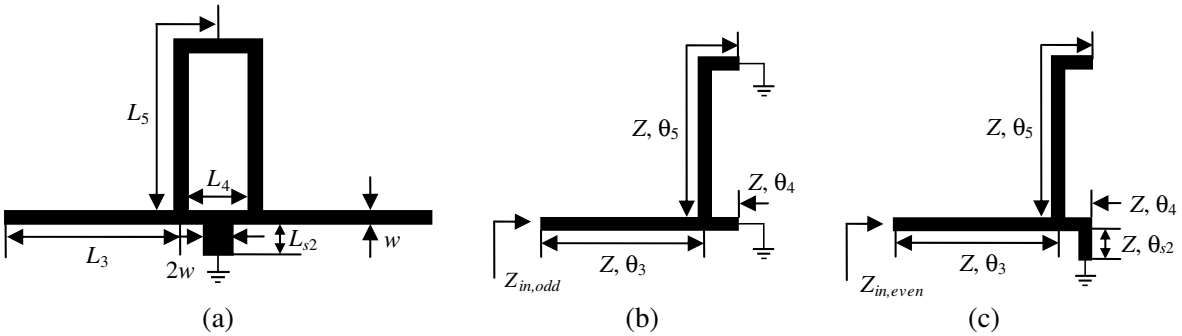

Figure 3. (a) Configuration of the TMR, (b) odd- and (c) even-mode equivalent circuits of (a).

$$\tan\theta = \infty \tag{9a}$$

$$2\tan\theta - \cot(\theta_4 + \theta_{s2}) = 0 \tag{9b}$$

And the odd-mode resonant frequencies can be extracted by Equation (8), whereas the even-mode ones can be deduced by Equation (9).

The solutions of Equation (8) is

$$f_{o3} = \frac{2f_{m2}}{\pi}\tan^{-1}\left[\frac{\cot(L_4\pi/\lambda_g) + \sqrt{\cot^2(L_4\pi/\lambda_g) + 4}}{2}\right] \tag{10a}$$

$$f_{o4} = \frac{2f_{m2}}{\pi}\tan^{-1}\left[\frac{\cot(L_4\pi/\lambda_g) - \sqrt{\cot^2(L_4\pi/\lambda_g) + 4}}{2}\right] \tag{10b}$$

However, f_{o3} is approximately f_{m2} when L_4 is very short whereas f_{o4} is about $2f_{m2}$ according to Equations (10a) and (10b). Therefore, only f_{o3} is considered for constructing the second passband.

The even-mode resonant frequencies can be obtained by solving Equation (9)

$$f_{e3} = f_{m2} \tag{11a}$$

$$f_{e4} = \frac{2f_{m2}}{\pi}\tan^{-1}\left[\frac{\cot((L_4 + 2L_{s2})\pi/\lambda_g)}{2}\right] \tag{11b}$$

It is notable from Equations (10) and (11) that the TMR exhibits triple-mode resonant characteristics (i.e., f_{o3}, f_{e3}, and f_{e4}). Equation (10b) reveals that f_{o3} is only affected by L_4, whereas Equation (11b) indicates that L_{s2} only influences f_{e4}. Therefore, the second wideband can be formed by shortening L_4 and $L_4 + 2L_{s2}$ according to Equations (10a) and (11b), respectively.

Figures 2(c) and (d) show the extracted resonant modes of the TMR with varied L_{s2} and L_4. It can be seen that f_5 can be controlled by L_{s2} independently, and both f_5 and f_6 decrease with the increase of L_4. These are consistent with the analysis mentioned above.

2.2. Filter Design

Based on the above analysis, a dual-wideband BPF centered at 2.34 and 3.46 GHz with fractional bandwidths of 25.6% and 21.4% is designed for WLAN/WiMAX applications. Figure 4 depicts the specific configuration of the proposed dual-wideband BPF it is composed of the QMR and TMR analyzed above and a pair of common feedlines. The two resonators are connected by a common via-hole. Also, the stubs are folded for the sake of a compact size.

The design procedure of the first passband using the QMR can be expressed as follows. First, determine L_1 and L_2 ($l_1 + l_2 + l_3$ and $l_4 + l_5 + l_6$ in Figure 4) by locating $f_{o1}(f_{e1})$ at the CF of the first passband f_{c1}. Second, shorten s and L_{s1} (s and l_{s1} in Figure 4) and make f_{o2} and f_{e2} approaching to f_{c1}. Then, f_{o1} and f_{e1} will split under weak coupling between the two loaded open-ended stubs. At last, f_{o1}, f_{o2}, f_{e1}, and f_{e2} can be allocated within the first passband after fine tuning, and the bandwidth can be tuned by controlling the positions of these four modes.

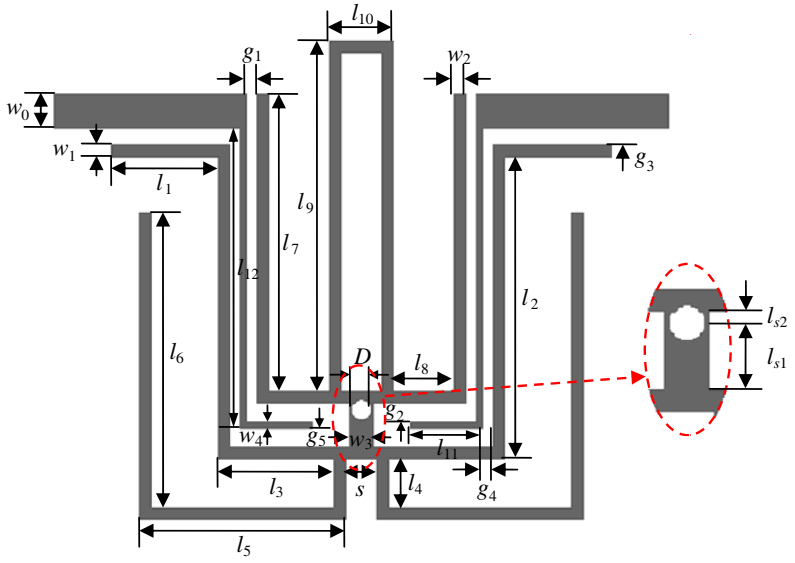

Figure 4. Configuration of the proposed dual-wideband BPF.

The design procedure of the second passband is similar to that of the first one. First, determine L_3 and L_5 ($l_7 + l_8$ and $l_9 + l_{10}/2$ in Figure 4) by locating f_{e3} at the CF of the second passband f_{c2}. Then, shorten L_4 and L_{s2} (l_{10} and l_{s2} in Figure 4) and make f_{o3} and f_{e4} approaching to f_{c2}. Finally, f_{o3}, f_{e3}, andf_{e4} can be distributed within the second passband after fine tuning, and the bandwidth can be adjusted by controlling the positions of these three modes.

After the two resonators are designed, the proposed dual-wideband BPF can be formed by connecting them with a common via-hole and feeding them with a pair of common input and output. The length of the feedlines are about quarter-wavelength at f_{c2}, and the coupling length between the QMR and the feedlines is tuned by l_1. Figure 5 compares the first, second, and dual passbands with the QMR, TMR, and both MMRs, respectively. It is noted that each resonator provides an individual wide passband and the dual-wideband performance can be obtained by combining these two resonators, which means the two passbands of the proposed filter can be controlled independently by tuning the design parameters of the corresponding resonator. These are consistent with the above analysis.

3. SIMULATED AND MEASURED RESULTS

For demonstration, a dual-wideband BPF prototype is designed, fabricated, and measured. The substrate used in this work has a dielectric constant of 3.38 a thickness of 0.508 mm, and a loss tangent of 0.0027. All simulation works are carried out by an electromagnetic (EM) simulator HFSS, and measurement works are performed with an Agilent's N5244A PNA. The optimal dimension parameters are as follows: $l_1 = 3.84$, $l_2 = 10.16$, $l_3 = 3.4$, $l_4 = 1.6$, $l_5 = 6.8$, $l_6 = 9.75$, $l_7 = 9.85$, $l_8 = 2$, $l_9 = 11.6$, $l_{10} = 2.14$, $l_{11} = 2.3$, $l_{12} = 10.36$, $l_{s1} = 1.23$, $l_{s2} = 0.23$, $w = 1.15$, $w_1 = w_2 = 0.4$, $w_3 = 0.8$, $w_4 = 0.2$, $g_1 = 0.13$, $g_2 = 1.06$, $g_3 = 0.4$, $g_4 = 0.1$, $g_5 = 0.2$, $s = 1$, and $D = 0.7$ (all in mm). The overall size is only $15.86 \times 16.28\,\text{mm}^2$, i.e., about $0.2 \times 0.21\lambda_g^2$, where λ_g is the guided wavelength at 2.34 GHz. The photograph of the fabricated filter is shown in the inset plot of Figure 6.

Figure 6 plots the simulated and measured results of the prototype filter, which indicates that the measured results agree well with the simulated ones. The first and second passbands, which CFs are 2.34 and 3.46 GHz, have measured minimum insertion losses (IL) of 0.84 and 1.21 dB with 3 dB fractional bandwidths (FBWs) of 25.6%, and 21.4%, respectively. The measured return losses (RL) are better than 16.9 and 15.8 dB. The isolation level between the two passbands is about 32.5 dB. Three transmission zeros can be observed at 1.34, 2.8 and 4.46 GHz in Figure 6: TZ_1 is created by the weak source-load coupling, TZ_2 is introduced by the loaded open-ended stubs of the QMR (L_2 in Figure 1(a)) when its length is about quarter-wavelength at TZ_2, and TZ_3 is generated due to the transversal signal

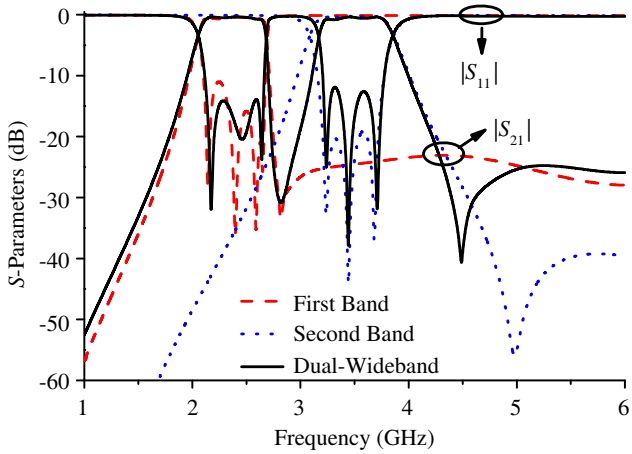

Figure 5. Simulated S-parameters of the first, second, and dual passbands with the QMR (dash line), TMR (dot line), and both MMRs (solid line).

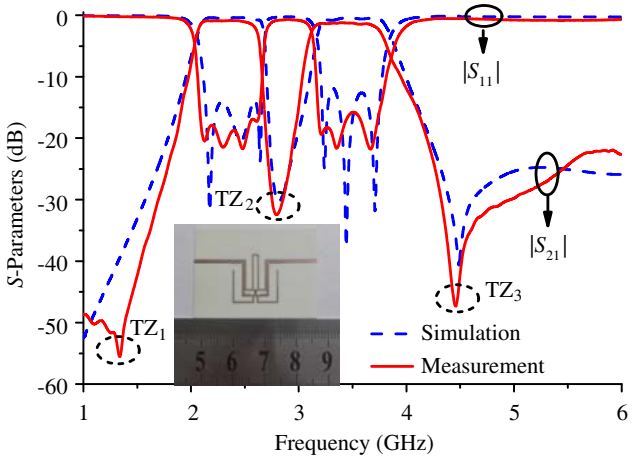

Figure 6. Simulated and measured results of the proposed dual-wideband BPF.

interference between the two signal paths of the TMR. These TZs improve skirt selectivity and band-to-band isolation level greatly.

Table 1 summarizes the comparison of the proposed filter with some previously reported works. The proposed dual-wideband BPF exhibits merits of compact size, wide bandwidths, low IL, good in-band and stop-band performance, high skirt selectivity, and independent control of CFs and FBWs. It is worth mentioning that the size of the proposed filter is about 80.4% reduction in comparison with [10].

Table 1. Comparison of the proposed dual-wideband BPF with other reported works.

Refs.	CF (GHz)	IL (dB)	RL (dB)	FBW (%)	Size ($\lambda_g \times \lambda_g$)
Filter 2 in [1]	2.35/5.05	1.64/2.9	17.7/11.6	16.6/13.5	N/A
Filter 4 in [2]	2.4/5.8	1.1/2.2	18.6/12.4	8/5	0.68×0.158
[5]	2.4/5.7	1.37/1.73	13/15	9.8/12	0.22×0.215
[10]	1.63/2.42	0.86/0.97	N/A	28.8/22.7	0.69×0.31
[12]	3.32/5.32	0.62/0.91	17/19	27.7/19.2	0.18×0.4
This work	2.34/3.46	0.84/1.21	16.9/15.8	25.6/21.4	0.2×0.21

4. CONCLUSION

In this letter, a novel compact dual-wideband BPF using two sets of MMRs, a quad-mode one (QMR) and a triple-mode one (TMR), is introduced and analyzed. The QMR consists of a main transmission line loaded with a short-ended stub and two open-ended stubs, and the TMR is composed of a main transmission line loaded with a square ring and a short-ended stub. Due to the symmetrical configurations, even-/odd-mode analysis is applied to explain their modal characteristics, which reveals that both of the proposed MMRs exhibit independently controllable resonant modes. By controlling the dimension parameters, each resonator forms an individual wide passband. Then, dual-wideband performance can be achieved by sharing a common via-hole and feeding them with a pair of common feedlines. The center frequency and bandwidth of each passband can be tuned separately by controlling the corresponding resonator. Good agreement between the simulated and measured results demonstrates the validity of the proposed dual-wideband BPF.

REFERENCES

1. Guo, L., Z.-Y. Yu, and L. Zhang, "Design of a dual-mode dual-band filter using stepped impedance resonators," *Progress In Electromagnetics Research Letters*, Vol. 14, 147–154, 2010.
2. Zhang, S. and L. Zhu, "Synthesis design of dual-band bandpass filters with $\lambda/4$ stepped-impedance resonators," *IEEE Trans. Microw. Theory Tech.*, Vol. 61, No. 5, 1812–1819, May 2013.
3. Li, J., S. S. Huang, and J. Z. Zhao, "Design of a compact and high selectivity tri-band bandpass filter using asymmetric stepped-impedance resonators (SIRs)," *Progress In Electromagnetics Research Letters*, Vol. 44, 81–86, 2014.
4. Luo, S., L. Zhu, and S. Sun, "A dual-band ring-resonator bandpass filter based on two pairs of degenerate modes," *IEEE Trans. Microw. Theory Tech.*, Vol. 58, No. 12, 3427–3432, 2010.
5. Chen, F.-C. and J. M. Qiu, "Third-order dual-band bandpass filter with controllable bandwidths using short stub-loaded resonators," *Progress In Electromagnetics Research Letters*, Vol. 32, 101–108, 2012.
6. Li, J., S. S. Huang, H. Wang, and J. Z. Zhao, "Compact dual-band bandpass filter using embedded center-grounded SIR and open-loop resonators," *Progress In Electromagnetics Research Letters*, Vol. 49, 9–14, 2014.
7. Chen, F. C., Q. X. Chu, Z. H. Li, and X. H. Wu, "Compact dual-band bandpass filter with controllable bandwidths using stub-loaded multiple-mode resonator," *IET Microw. Antennas Propag.*, Vol. 6, No. 10, 1172–1178, 2012.
8. Chin, K.-S. and J.-H. Yeh, "Dual-wideband bandpass filter using short-circuited stepped-impedance resonators," *IEEE Microw. Wireless Compon. Lett.*, Vol. 19, No. 3, 155–157, 2009.
9. Zhou, J.-G., W.-J. Feng, and W.-Q. Che, "Dual-wideband bandpass filter using T-shaped structure based on transversal signal-interaction concepts," *Electron. Lett.*, Vol. 48, No. 24, 1539–1540, 2012.
10. Xu, J. and W. Wu, "Miniaturised dual-wideband bandpass filter using novel dual-band coupled-line sections," *Electron. Lett.*, Vol. 49, No. 18, 1162–1163, 2013.
11. Li, J., S.-S. Huang, and J.-Z. Zhao, "Compact dual-wideband bandpass filter using a novel penta-mode resonator (PMR)," *IEEE Microw. Wireless Compon. Lett.*, Vol. 24, No. 10, 668–670, 2014.